

# Integrative Biology

Accepted Manuscript



This is an *Accepted Manuscript*, which has been through the RSC Publishing peer review process and has been accepted for publication.

*Accepted Manuscripts* are published online shortly after acceptance, which is prior to technical editing, formatting and proof reading. This free service from RSC Publishing allows authors to make their results available to the community, in citable form, before publication of the edited article. This *Accepted Manuscript* will be replaced by the edited and formatted *Advance Article* as soon as this is available.

To cite this manuscript please use its permanent Digital Object Identifier (DOI®), which is identical for all formats of publication.

More information about *Accepted Manuscripts* can be found in the [Information for Authors](#).

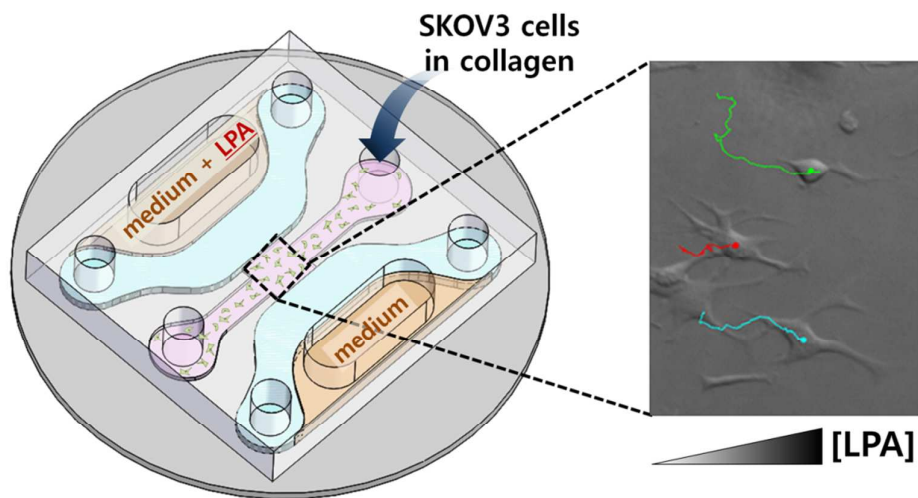
Please note that technical editing may introduce minor changes to the text and/or graphics contained in the manuscript submitted by the author(s) which may alter content, and that the standard [Terms & Conditions](#) and the [ethical guidelines](#) that apply to the journal are still applicable. In no event shall the RSC be held responsible for any errors or omissions in these *Accepted Manuscript* manuscripts or any consequences arising from the use of any information contained in them.

## Table of Contents

### RhoA and Rac1 play independent roles in lysophosphatidic acid-induced ovarian cancer chemotaxis

Hyundoo Hwang<sup>a,†</sup>, Eung-Kyun Kim<sup>a,†</sup>, Juhee Park<sup>a</sup>, Pann-Ghill Suh<sup>a,\*</sup>, Yoon-Kyoung Cho<sup>a,\*</sup>

RhoA and Rac1 signaling pathways involve in controlling directionality and velocity of the cells, respectively, in lysophosphatidic acid-induced chemotaxis of SKOV3 ovarian cancer cells.



## **RhoA and Rac1 play independent roles in lysophosphatidic acid-induced ovarian cancer chemotaxis**

Hyundoo Hwang<sup>a‡</sup>, Eung-Kyun Kim<sup>a‡</sup>, Juhee Park<sup>a</sup>, Pann-Ghill Suh<sup>a\*</sup>, Yoon-Kyoung Cho<sup>a\*</sup>

### ***Insight, innovation, integration***

Roles of small GTPases in lysophosphatidic acid-induced chemotaxis of SKOV3 ovarian cancer cells were first investigated using a novel microfluidic assay platform. Real-time tracking of individual cells in the rapid-prototyped multilevel microfluidic devices provided us substantial quantitative information about the chemotaxis of the cells under a linear and stable concentration gradient. This integrative study of cellular chemotaxis would provide us new biological insights, which could not be obtained through the traditional tools for cell migration assays.

## ARTICLE

## RhoA and Rac1 play independent roles in lysophosphatidic acid-induced ovarian cancer chemotaxis

Cite this: DOI: 10.1039/x0xx00000x

Received 00th January 2012,  
Accepted 00th January 2012

DOI: 10.1039/x0xx00000x

www.rsc.org/

Hyundoo Hwang<sup>a‡</sup>, Eung-Kyun Kim<sup>a‡</sup>, Juhee Park<sup>a</sup>, Pann-Ghill Suh<sup>a\*</sup>, Yoon-Kyoung Cho<sup>a\*</sup>

Lysophosphatidic acid (LPA), which is a bioactive phospholipid existing at high level in ascites and plasma of ovarian cancer patients, is known as involving in cell survival, proliferation, adhesion, and migration. Small guanosine triphosphatases (GTPases) such as RhoA and Rac1 are intracellular signaling molecules which affect morphology and chemotactic behavior of cells. In this research, we first investigated roles of RhoA and Rac1 in the LPA-induced chemotaxis of SKOV3 human ovarian cancer cells using a multilevel microfluidic platform. The multilevel microfluidic device was fabricated by a rapid prototyping method based on soft lithography using multi-layered adhesive tapes. This platform allows us to conduct the on-chip chemotaxis assays in conventional biology laboratories without any huge and expensive equipment for fabrication and fluidic manipulation. Based on image-based analysis of single cell trajectories in the microfluidic device, the chemotaxis of SKOV3 cells could be quantitatively analyzed in two independent parameters – migration speed and directional persistence. Inhibition of the RhoA/ROCK pathways reduced the directional persistence, not the migration speed, of the cells, while only the migration speed was decreased when the activity of Rac1/PAK pathways was suppressed. These results suggest that RhoA and Rac1 signaling pathways potentially play independent roles in the chemotactic migration of SKOV3 ovarian cancer cells in the linear and stable LPA concentration gradient. Our microfluidic platform would provide a rapid, low cost, easy-to-use, and versatile way for research of cancer cell migration which is crucial for tumor metastasis.

### Introduction

Ovarian cancer, the most lethal gynecologic malignancy in the United States and other countries, is a highly metastatic disease spreading beyond the ovary into other organs. Lysophosphatidic acid (LPA), which is known as involving in cell survival, proliferation, adhesion, and migration,<sup>1</sup> exists at high levels in ascites and plasma of ovarian cancer patients.<sup>2, 3</sup> Thus its potential role in ovarian cancer metastasis has been actively studied during the past few decades.<sup>4-8</sup> LPA promotes the expression of proteolytic enzymes such as matrix metalloproteinases (MMPs) and plasminogen activators, which dissolve extracellular matrix, allowing cell invasion.<sup>9-12</sup> LPA also down regulates tissue inhibitors of MMPs, which play functional role as negative regulators in LPA-induced cell invasion.<sup>13</sup> Interleukin-8 and vascular endothelial growth factor receptor also involve in LPA-induced cell invasion.<sup>14, 15</sup>

LPA also activates Rho family of small guanosine triphosphatases (GTPases) such as RhoA and Rac1 in a variety of manners.<sup>16-19</sup> Through a plenty of studies based on various types of cells and extracellular stimuli, it has been well-known that the Rho-family GTPases play significant roles in regulation

of cytoskeletal structure, cellular adhesion, and migration.<sup>20-24</sup> Even in ovarian cancer cells, the LPA-induced activation of Rho GTPase pathways induces actin cytoskeleton reorganization, focal adhesion assembly, and cell migration.<sup>16-19, 25</sup> A recent study showed that the LPA-induced Rho activation is also implicated in expression of proteolytic enzymes and ovarian cancer cell invasion in an nuclear factor- $\kappa$ B-dependent manner.<sup>26</sup>

In general, RhoA is required for generation of contractile force and tail retraction, whereas Rac controls extension of lamellipodium and formation of new adhesions.<sup>22-24</sup> However, it has been observed that specific functions of the Rho-family GTPases on cell migration vary depending on cell types, stimuli, and expression level. For instances, in colony-stimulating factor-1-induced chemotaxis of macrophages, RhoA and Rac1 affect both migration speed and directional persistence of cell invasion, whereas Cdc42 affects only directional persistence, but is not essential for cellular locomotion.<sup>27</sup> In human fibroblasts, suppression of RhoA or Cdc42 expression decreases migration speed, but does not affect directional persistence of cell invasion, while suppression of Rac1 increases directional persistence of cell migration in N-formyl-methionyl-leucyl-phenylalanine-induced chemotaxis.<sup>28</sup> In

human umbilical vein endothelial cells, RhoA and Rac1, but not Cdc42, are involved in shear stress-induced orientation. Here RhoA is involved in shear stress-induced cell polarization, but does not affect migration speed, whereas Rac1 and Cdc42 are required for maintenance of migration speed.<sup>29</sup> However, it has been largely unexplored how such the Rho-family GTPases function to regulate the LPA-induced chemotactic migration of ovarian cancer cells.

In order to gain insight into role of molecular signaling pathways related to Rho-family GTPases such as RhoA and Rac1 in LPA-induced chemotaxis of human ovarian cancer cells, we developed a microfluidic platform which allows integrative analysis of cellular movements under a stable molecular concentration gradient across a 3-dimensional (3D) hydrogel structure in a simple and low-cost manner. The microfluidic device is composed of multilevel microchannels, which are laterally open to adjacent channels having different heights. The multilevel microfluidic device provides a simple and robust way to form hydrogel microstructures at specific compartments by capillary force-driven passive pumping.<sup>30</sup> The unique operational regime in multilevel microchannels offers additional advantage of an opportunity to exclude excess peripheral equipments such as syringe pumps and tubings, as well as complicated microfabrication processes, which require expensive clean room facilities. Besides, our device allows us to form reproducible, well-controlled, and physiologically relevant microenvironments, as like most of the microfluidic devices which have been previously developed for studying cellular chemotaxis.<sup>31-35</sup>

In the microfluidic chemotaxis assays, one can trace individual cells straightforwardly, thus more detailed information related to the cellular behavior can be obtained than in the traditional methods. While the number of cells migrated through the porous membrane after a certain time is the only factor for quantifying the chemotactic ability of the cells in the traditional Boyden chamber assay, tracking cellular trajectories in the microfluidic channels offers spacious data collections including the velocity, the directionality, and the morphological phenotypes of the cells simultaneously.<sup>36, 37</sup>

In this research, role of RhoA and Rac1 in the LPA-induced chemotaxis of human ovarian cancer cells was studied by tracing the migration of the cells in the hydrogel-loaded multilevel microchannels. The SKOV3 cells were treated with selective inhibitors of the effector proteins to suppress their activity, and the changes in their speed or persistence were analyzed based on their trajectory data. Through the live cell tracking-based analysis, we found that inhibition of RhoA and its downstream effector suppresses directionality of the cells, not their velocity, while inhibition of Rac1 and its downstream effector decreases only their migration speed in LPA-induced chemotaxis.

## Materials and method

### Chemicals and reagents

LPA (1-oleoyl-2-hydroxy-*sn*-glycero-3-phosphate) was purchased from Avanti Polar Lipids, Inc. (Alabaster, AL). Anti-Rac1 and anti-RhoA antibodies were purchased from Santa Cruz Biotechnology, Inc. (Santa Cruz, CA). *Clostridium botulinum* C3 exoenzyme purchased from Enzo Life Sciences, Inc. (Farmingdale, NY). Y-27632, NSC23766, and IPA-3 were purchased from Tocris Bioscience (Bristol, United Kingdom). RPMI-1640 and fetal bovine serum (FBS) were purchased from Hyclone (Logan, UT). Antibiotic/antimycotic solution was

purchased from Gibco (Grand Island, NY). PureCol (3 mg/ml purified bovine collagen solution, ~97% type I collagen and 3% type III collagen) was purchased from Advanced BioMatrix (San Diego, CA). Low gelling temperature agarose, fluorescein-5-thiocyanate (FITC), and Hoechst 33342 were purchased from Sigma-Aldrich Corp. (St. Louis, MO). Polydimethylsiloxane (PDMS) and curing agent (Sylgard 184 Silicone Elastomer Kit) were purchased from Dow Corning (Midland, MI).

### Cell culture and transfection

Human ovarian cancer SKOV3 cell lines were purchased from the American Type Culture Collection (Manassas, VA). Cells were cultured in RPMI 1640 medium with 10% FBS, 100 units/ml of penicillin, and 100 µg/ml of streptomycin inside a humidified 5% CO<sub>2</sub> incubator at 37°C. For transient transfection (dominant negative flag-N17RhoA or flag-N17Rac1), Lipofectamine 2000 (Invitrogen, Madison, WI) reagent was used according to the manufacturer's instructions.

### Rho GTPases activation assay

The activity of RhoA and Rac1 was measured using the GST-Rho binding domain of Rhotekin (RBD) or GST-Rac binding domain of Pak (PBD) bound to Glutathione Sepharose 4B beads. Cells were lysed in lysis buffer (50 mM Tris, pH 7.5, 10 mM MgCl<sub>2</sub>, 0.5 M NaCl, and 1% Triton X-100), and the lysates were incubated with GST-RBD or GST-PBD beads at 4°C for 40 min. The beads were collected by centrifugation and washed three times with washing buffer (25 mM Tris-HCl, pH 7.6, 1 mM DTT, 30 mM MgCl<sub>2</sub>, 40 mM NaCl, and 1% v/v Nonidet P-40). Proteins were eluted from beads by boiling in 2X sample buffer for 5 min. The precipitates were analyzed with antibodies specific for RhoA or Rac1. To equalize the cellular proteins in each sample, total cell lysates were also run on gels and subjected to Western blot analysis.

### Immunoblot analysis

Cells were serum-starved for overnight prior to treatment with the indicated agents. Whole cell lysates were prepared in lysis buffer, as previously described.<sup>17</sup> Lysates were then centrifuged at 14,000 × g for 10 min at 4°C. Supernatants were electrophoresed on 8 % sodium dodecyl sulfate polyacrylamide gel electrophoresis gels and transferred to nitrocellulose membranes. Membranes were incubated overnight at 4°C with primary antibodies and then washed three times in Tris-buffered saline with 0.1 % Tween 20 prior to 1 h incubation with horseradish peroxidase-conjugated secondary antibodies (Gaithersburg, MD) at room temperature. Proteins were then detected via ECL reagents (Amersham Biosciences, Buckinghamshire, UK).

### Transwell cell migration analysis

Cell migration was evaluated using a modified Boyden chemotaxis chamber (Neuroprobe Inc., Gaithersburg, MD). Porous filters (8 µm) were coated by passive absorption of type I collagen (Sigma-Aldrich Corp.) by incubation with 20 µg/ml collagen overnight at 4°C. Medium containing LPA (0 - 10 µM) was placed in the bottom wells of the chamber. Cells were trypsinized and washed, and then resuspended in media. The upper chamber was loaded with cells (2 × 10<sup>4</sup>) and allowed to migrate for 4 h. Non-migrating cells were removed from the

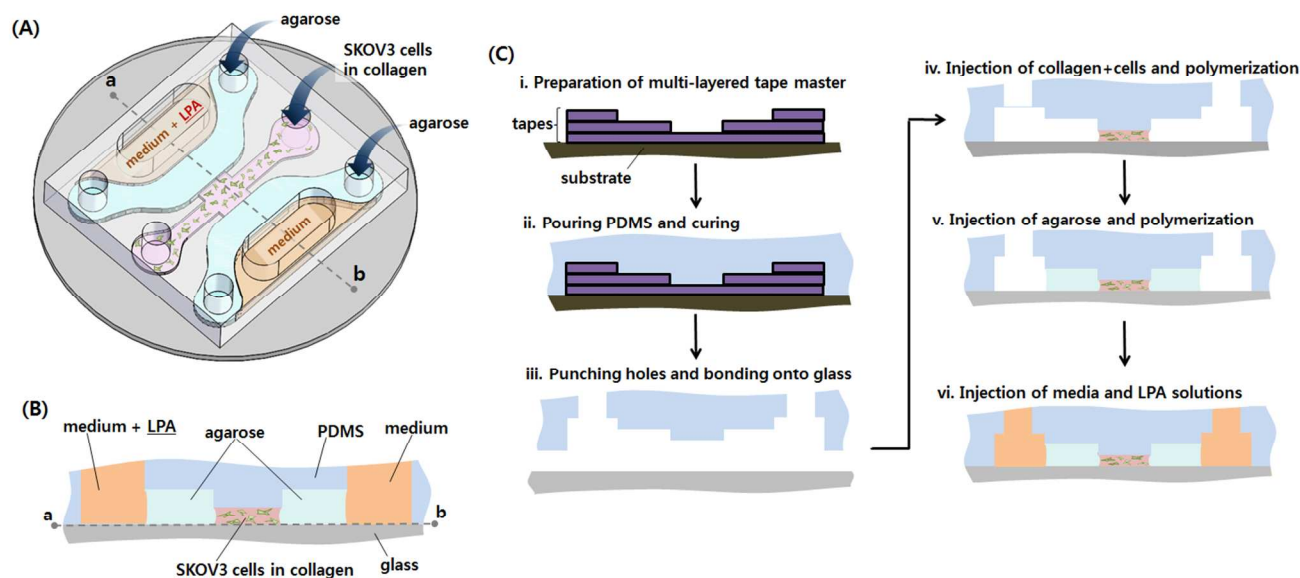


**Fig. 1** Microfluidic device for cell migration assays. **(A)** Schematic diagram of a multilevel microfluidic device. **(B)** Cross-sectional view of the microfluidic device along the dashed line (a—b) shown in (A). **(C)** Fabrication process of the microfluidic device for 3D cell migration studies.

upper chamber with a cotton swab, whereas migrating cells adherent to the underside of the filter were fixed with 4% paraformaldehyde, permeated with 0.2% triton X-100 and stained with Hoechst 33342 solution. The migrated cells were photographed and quantified by fluorescent microscopy at a magnification of  $100\times$  by counting the stained cells from three randomly chosen high power fields.

### Wound healing assay

SKOV3 cells ( $2 \times 10^5$ ) were grown for 24 h in a type I collagen-coated 96-well Essen BioScience ImageLock microplate in a standard  $\text{CO}_2$  incubator. Wounds were made precisely by the 96-pin Wound-Maker provided with the IncuCyte FLR.<sup>38</sup> After washing thoroughly with PBS to remove the detached cells, the cells were placed in the IncuCyte FLR with media containing vehicle or LPA. The wound images were automatically acquired by IncuCyte FLR (Essen Bioscience) from the incubator at 1-h intervals. The kinetics of the relative wound density (RWD) was analyzed by IncuCyteTM software.

### Design and fabrication of microfluidic devices

The microfluidic device for on-chip chemotaxis assays was fabricated using a rapid prototyping method based on adhesive tapes (Fig. 1C).<sup>30</sup> A microfluidic device, which has three different levels — a  $100\ \mu\text{m}$ -height main channel, two  $200\ \mu\text{m}$ -height side-channels adjacent to the main channel, and two  $300\ \mu\text{m}$ -height side-chambers —, was fabricated for the experiment. The width of all the channels was fixed as 1 mm. The 3-level microfluidic device could be fabricated by using triple-layered adhesive tapes as a master for molding PDMS. The tapes were cut into a desired design for each level using a cutting plotter (CE3000-60; Graphtech Corp., Japan) and stacked layer-by-layer for constructing multilevel structures. A 10:1 mixture of the PDMS prepolymer and the curing agent was poured onto the tape master, followed by curing in an oven at  $65^\circ\text{C}$  for 2 h. The PDMS was peeled off from the master, diced into

individual chips, and holes were punched. The PDMS structure was bonded onto a glass coverslip of 25 mm diameter after an oxygen plasma treatment of both the PDMS and the glass surfaces.

### On-chip cell migration assay

Prior to the experiment, the devices were sterilized with 70% ethanol under a laminar flow hood with ultraviolet exposure for more than 30 min. The collagen gel containing SKOV3 cells at density of  $1 \times 10^6$  cells/ml was injected into the  $100\ \mu\text{m}$ -height main channel of the device, followed by the polymerization in a 5%  $\text{CO}_2$ ,  $37^\circ\text{C}$  incubator for 50 min. Then 1% agarose solution, generated by heating the low gelling temperature agarose in phosphate-buffered saline (PBS) solution, was injected into the  $200\ \mu\text{m}$ -height side-channels adjacent to the main channel. After gelation of the agarose solution at the room temperature,  $10\ \mu\text{M}$  LPA in RPMI-1640 medium and blank RPMI-1640 medium were loaded into each  $300\ \mu\text{m}$ -height side-chamber, respectively. Finally, the devices were mounted in a custom-built live cell chamber, in which 6 devices could be simultaneously processed under controlled temperature and  $\text{CO}_2$ , on a stage of an inverted microscope equipped with motorized stage (IX81-ZDC; Olympus Corp., Japan) and an EMCCD camera (Andor iXon 897; Till Photonics GmbH, Gräfelfing, Germany). After 2 h incubation, during which the linear gradient of LPA across the gel was formed and the cells were stabilized, time-lapsed images of the cell movements were taken in bright field every 5 min using a  $10\times$  objective for a total length of 6 h.

For inhibition experiments, the inhibitors were added to the collagen gel prior to mixing with cells. The concentrations of the inhibitors —  $10\ \text{nM}$  C3 exoenzyme,  $10\ \mu\text{M}$  Y-27632,  $2\ \mu\text{M}$  NSC23766, and  $2\ \mu\text{M}$  IPA-3 — were fixed on the basis of preliminary experiments for investigating the dose-dependency and the cell viability. In the case of C3 exoenzyme, the LPA solution was added after 24 h incubation exceptionally.

### Cell tracking analysis

The time-lapsed images were automatically analyzed using MetaMorph software (Molecular Devices, LLC, Sunnyvale, CA) to obtain the trajectories of SKOV3 cells in the collagen gel. The collected data was utilized for calculating the migratory information — velocity and directional persistence — of the cells using MATLAB (Mathwork Co., Natick, MA). Statistical analysis was conducted using Prism (Graphpad, La Jolla, CA).

### Fluorescent dye experiment

To visualize the generation of chemical concentration gradient across the gels, an FITC solution was loaded into one side-chamber and its distribution was observed according to the time. A confocal microscopy (LSM700; Carl Zeiss MicroImaging GmbH, Germany) was used for observing the distribution of fluorescence dyes across the gels. The fluorescence intensity profiles were measured using ImageJ software.

### Simulation study

The temporal change of the LPA distribution in the microchannels was simulated using COMSOL Multiphysics 4.2 (COMSOL Inc., Burlington, MA). The distribution of LPA molecules within the hydrogels was estimated in the ranges from 0 to 8 h after loading the LPA solution. Each hydrogel area was modeled as a spatially uniform porous phase and the diffusion coefficient of LPA molecules was assumed to be  $3 \times 10^{-10} \text{ m}^2/\text{s}$ . In addition, we assumed that there is neither flux across the PDMS walls nor evaporation during the diffusion process and the LPA source is limited without perfusion.

### Statistical analysis

The data were analyzed using Student's *t*-test. All of the experiments presented in the present study were repeated at least three times.  $P < 0.05$  was considered statistically significant.

## Results

### Microfluidic 3D cell migration assays

A schematic diagram of a microfluidic device for 3D cell migration assays is shown in Fig. 1A. The PDMS device has microchannels of three different levels (Fig. 1B). The multilevel microfluidic device was fabricated by a rapid prototyping method based on soft lithography using multi-layered adhesive tapes (Fig. 1C).<sup>30</sup> A collagen gel containing human ovarian cancer SKOV3 cells was loaded in the shallowest main channel, then the side-channels adjacent to the main channel were filled with agarose gels. The agarose gels increase the mechanical stability of the gel scaffolds for long-term migration experiments. To form a concentration gradient of LPA across the gels, a  $10 \mu\text{M}$  LPA buffer and a blank buffer were loaded into two side-chambers, respectively.

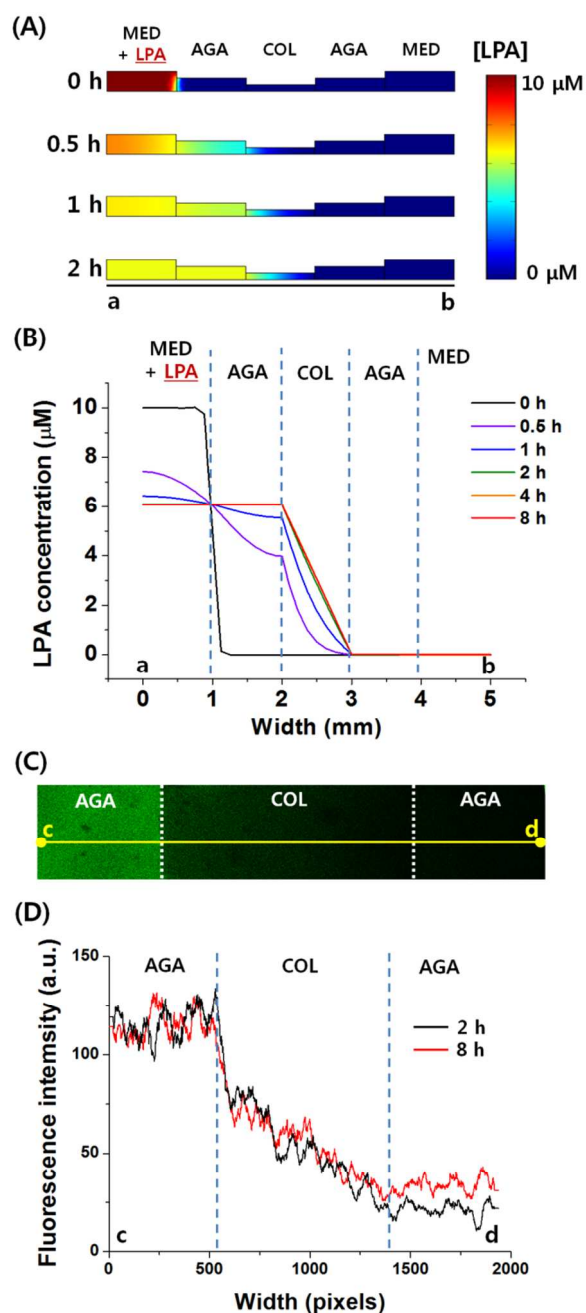


**Fig. 2** Generation of linear chemical concentration gradient. (A) Simulation results showing the LPA distribution in the microfluidic channels against the time. (B) Plot showing the temporal change of LPA concentration profile across the microchannels (a—b) shown in (A). (C) Confocal microscopic image showing the distribution of fluorescent dye across the gels. (D) Fluorescence intensity profiles along the solid line (c—d) shown in (C) at 2 h and 8 h after loading the dye solution. (COL, collagen; AGA, agarose; MED, medium; LPA, lysophosphatidic acid)

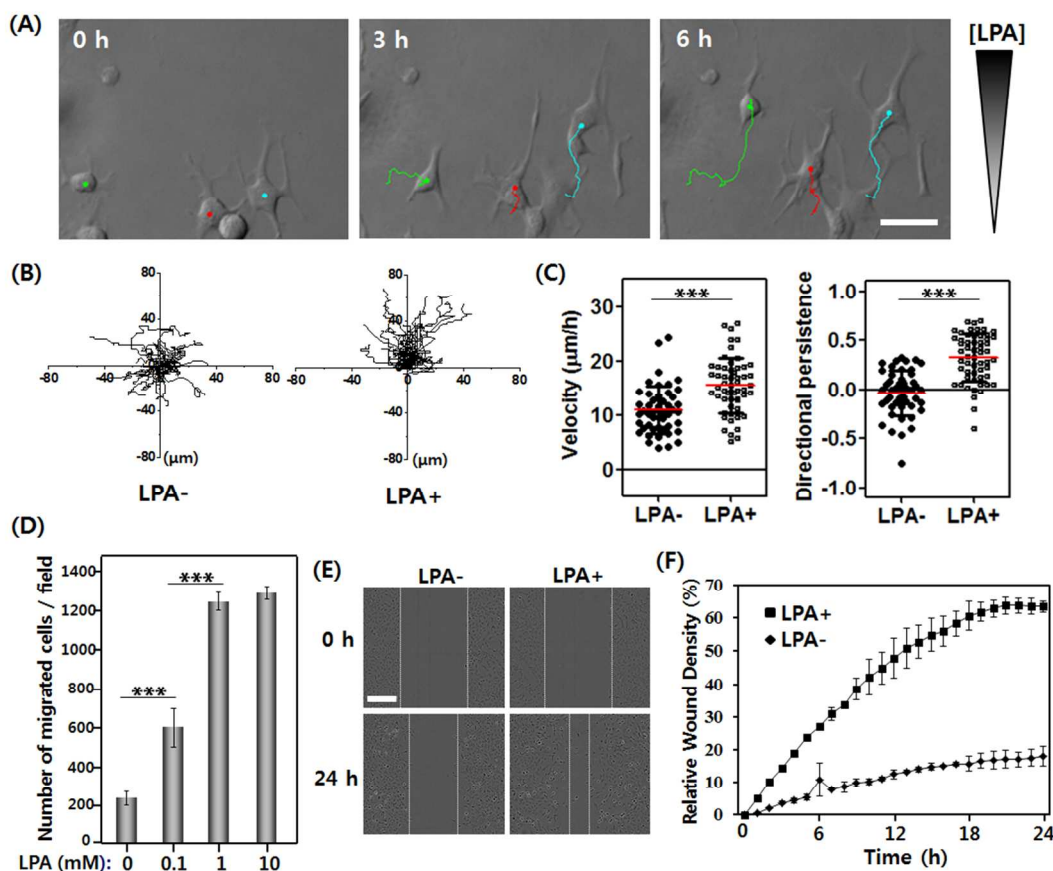


**Fig. 3** LPA-induced migration of SKOV3 cells (A) Time-lapsed images of SKOV3 cells migrating along the concentration gradient of LPA in the collagen gel. Scale bar: 50  $\mu\text{m}$ . (B) Trajectories of SKOV3 cells without (left) and with (right) LPA concentration gradient. (C) Migrational speed (left) and directional persistence (right) of SKOV3 cells calculated from the trajectory data. (D) Transwell analysis of LPA-induced migration of SKOV3 cells. \*\*\* $p < 0.0001$ . (E) Time-lapsed images of SKOV3 cells in wound healing assay without (left) and with (right) LPA. Scale bar: 300  $\mu\text{m}$ . (F) Temporal change of relative wound density against presence of LPA.

### Generation of linear concentration gradient within a gel

Prior to conduct on-chip chemotaxis assays, we determined the concentration gradient formed across the gels. According to the result of finite element analysis, the LPA molecules were diffused across the gels toward the other side of the device and formed a concentration gradient across the collagen gel within 2 h (Fig. 2A). The concentration gradient across the collagen gel was linear from 0 to 6  $\mu\text{M}$  and stable during more than 6 h as shown in Fig. 2B. Although there are 1% agarose gels adjacent to the cell-laden collagen gel, the linear concentration gradient was formed only within the collagen gel compartment. This might be due to rapid diffusion of the molecules across the agarose gel, which has relatively larger pore size than that of the collagen gel.<sup>39</sup> The chemical concentration gradient across the gels was also experimentally visualized with fluorescent dyes (Fig. 2C). To agree with our expectation, a concentration gradient of the fluorescent dye was formed across the collagen gel within 2 h, and maintained its linear profile for more than 6 h as shown in Fig. 2D. Thus, we could apply this microfluidic platform to investigate migration of human ovarian cancer cells under the linear LPA concentration gradient in 3D extracellular matrix microenvironment.

### Both migration speed and directional persistence of SKOV3 cells increase in LPA gradient

SKOV3 human ovarian cancer cells showed chemotactic migration when they exposed to the linear gradient of LPA concentration gradient in the collagen gel as shown in Fig. 3A. For quantitative analysis of cellular behavior, positions of individual cells were tracked every 5 min for 6 h. Their trajectories are plotted in Fig. 3B. Here the cell tracking began 2 h after loading the media, during which the LPA concentration gradient across the cell-laden collagen gel became linear and the cells began to sprout. The trajectory data was utilized for post-analyses to calculate the migration characteristics of the cells. Here we could obtain the average migration speed,  $V$ , and the directional persistence,  $P$ , of the cells through the calculation as follows:

$$V = S/t,$$

$$P = D/S,$$

where  $S$  is the total distance that cells migrated;  $t$  is the time; and  $D$  is the net cellular displacement along the gradient axis. According to the quantitative analyses, both the average migration speed and the directional persistence of SKOV3 cells significantly increased in the appearance of LPA gradient (Fig. 3C). To verify the reliability of our platform and to ascertain

how the results that we obtained in the on-chip experiments are reflected in the traditional assays that many researchers have widely used, we also conducted the traditional cell migration assays using Boyden chamber. According to the results from the experiments where the concentration of LPA was varied, the more number of cells migrated as the LPA concentration increased (Fig. 3D). Although such the endpoint assays do not allow of any detailed information regarding individual cell behaviors such as trajectories, mobility, and directionality, the enhanced migration behavior of SKOV3 cells towards the LPA source could at least be confirmed. The conventional wound healing assays were also performed to investigate changes in the growth and the migration properties of SKOV3 cells in response to LPA. According to the results shown in Fig. 3E and 3F, the SKOV3 cells showed significantly higher wound healing rate in response to the LPA. Considering to these results, we can therefore conclude that LPA increases both the velocity and the directionality of ovarian cancer cells. However, the underlying mechanisms are still poorly understood.

### RhoA and Rac1 play independent roles in LPA-induced chemotaxis of SKOV3 cells

Rho-GTPases are well-known as regulators of cytoskeleton rearrangement and cell migration.<sup>21</sup> It has been reported that LPA activates RhoA through Rho-specific guanine nucleotide-exchange factors (GEFs) that promote RhoA-GTP accumulation.<sup>40</sup> LPA also activates Rac and thereby promotes cell spreading, lamellipodium formation and cell migration.<sup>41</sup> Thus, we examined the effect of LPA on the activation of Rho-GTPases in SKOV3 cells. According to the Rho-GTPases activation assays, LPA activated both RhoA and Rac1 as early as 30 s and peaked at 2 min (Fig. 4).

To investigate the specific roles of RhoA and Rac1 in the LPA-induced chemotaxis of SKOV3 human ovarian cancer cells, analyses using the microfluidic devices and the live cell tracking method were carried out. Here, the SKOV3 cells were treated with selective inhibitors in the microfluidic device to selectively suppress the activation of each protein and their downstream effectors, and then we analyzed the changes in their chemotaxis under the LPA concentration gradient. In addition, the SKOV3 cells expressing dominant-negative RhoA and Rac1 mutants were also examined.

When the SKOV3 cells were treated with C3 exoenzyme, a selective Rho inhibitor, they showed significant decrease in the

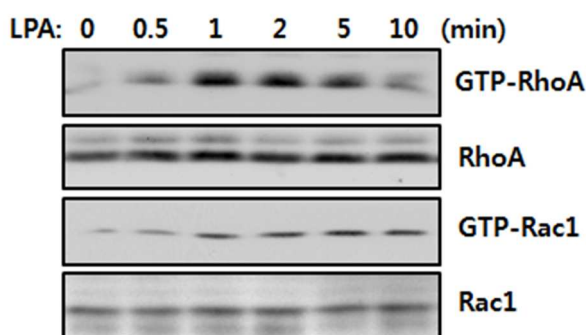


**Fig. 4** LPA induces activation of RhoA and Rac1. SKOV3 cells were stimulated for the indicated times with 10  $\mu$ M LPA under serum-free conditions. Total cell lysates were prepared and subjected to immunoblot analysis using specific antibodies against RhoA and Rac1.

LPA-induced activation of RhoA as shown in Fig. 5A. According to the on-chip experiments, the directional persistence of the SKOV3 cells was significantly decreased by the pretreatment with 10 nM C3 exoenzyme, while their average migration speed was not changed in comparison with the control without any inhibitors (Fig. 5B). When the cells were treated with 10  $\mu$ M Y-27632, a selective inhibitor of Rho-associated protein kinase (ROCK) which is known as a downstream effector of RhoA, they also lost their directionality of migration while their migration speed was retained, as like the C3 exoenzyme-treated cells (Fig. 5C). We also confirmed the effect of RhoA using RhoA dominant-negative cells (Fig. 5D). The directional persistence of the RhoA dominant-negative mutants was remarkably decreased, but the migration speed was not, as shown in Fig. 5E. Therefore, these results indicate that activation of RhoA is associated with the directional persistence of SKOV3 cells in LPA-induced chemotaxis.

We also investigated the role of Rac1 with the same approach. Interestingly, when we treated the SKOV3 cells with 2  $\mu$ M NSC23766, which selectively inhibits the LPA-induced activation of Rac1 (Fig. 6A), the average migration speed became significantly slower while the directional persistence was retained as shown in Fig. 6B. Such the chemotactic behavior, where only the migration speed was significantly decreased, was also shown in the addition of 2  $\mu$ M IPA-3, which is a selective inhibitor of p21-activated kinase (PAK), a downstream effector of Rac1 (Fig. 6C). In addition, the Rac1 dominant-negative cells also showed slower migration speed compared to the control, while they still maintained the directional persistence as shown in Fig. 6D and Fig. 6E. Taken together, these results demonstrate that the LPA-induced activation of Rac1 and its downstream effector dominantly governs the migration speed of the cells in the LPA-induced chemotaxis of SKOV3 cells, while the activation of RhoA and its downstream effector acts a dominant role in the directional persistence of the cells.

### Discussion and conclusion

In this research, the roles of RhoA and Rac1 in the LPA-induced chemotaxis of SKOV3 human ovarian cancer cells were investigated. It has been known that LPA activates both RhoA and Rac1 through GEFs, promoting rearrangement of cytoskeleton and cell migration,<sup>40, 41</sup> as consistent with our experimental results. However, it has not yet been clearly revealed to affecting which component of cell migration, velocity or directionality, through the activation of RhoA or Rac1 in the LPA-induced ovarian cancer chemotaxis. In this study, we applied real-time cell tracking and microfluidic technologies to map the role of intracellular signaling pathways to the migration patterns of SKOV3 cells in LPA-induced chemotaxis. We could quantify the chemotactic migration of SKOV3 cells in two independent parameters – migration speed and directional persistence – based on the image-based analysis of individual cell trajectories in microfluidic devices. The cells were pretreated with specific inhibitors of each protein in the microfluidic device before being exposed to the linear LPA gradient. The experiments with dominant negative cells were also conducted. According to the results, inhibition of RhoA/ROCK pathway in SKOV3 resulted in decrease of the directional persistence in the LPA-induced chemotaxis, while it did not affect the migration speed. When Rac1/PAK pathway

was inhibited, only the migration speed, not the directional persistence, decreased.

It has been known that Rho acts to regulate the contraction of cell body,<sup>42</sup> which sounds as a process determining the velocity of the migrating cells. However, our results show that RhoA/ROCK pathways are required for the directional movement of SKOV3 cells in the LPA-induced chemotaxis, not for the maintenance of the migration speed. It might be due to some alternative roles of RhoA such as focal adhesion assembly which is a part of major processes deciding the direction of the cells at the initial step in migration. In fact, it has also been known that RhoA induces the expression of matrix metalloproteinase(MMP)-9 at lamellipodial focal complexes in human microvascular endothelial cells<sup>43</sup> as well as the assembly of stress fibers and focal adhesions in human ovarian cancer cells<sup>18</sup> and fibroblasts.<sup>44</sup> Rac has been known to activate actin-related proteins 2/3 required for the formation of lamellipodium extension, which can be considered as very initial step to decide the direction of the migrating cells.<sup>45, 46</sup> On the other hand, it has also been reported that Rac induces expression of collagenase-1 in rabbit synovial fibroblasts<sup>47</sup> and MMP-2 in HT1080 fibrosarcoma cells.<sup>48</sup> Therefore, these functions including the protrusion at leading edge and the proteolysis may affect the migration speed of the cells in the 3D collagen structure, supporting our experimental results. Taken together, the selective inhibition of Rac1/PAK pathway might suppress the formation of lamellipodium or the expression of proteolytic enzymes, while the focal adhesion assembly might be still regulated by RhoA, resulting in the slowed directional migration of ovarian cancer cells under the LPA gradient. In the selective inhibition of RhoA/ROCK, the assembly of focal adhesions or the expression of proteolytic enzymes at the

lamellipodial regions might be delocalized, while Rac1 controls the formation of protrusion at leading edges or the globalized expression of proteolytic enzymes, resulting in random migration of the cells. Although the detailed mechanisms of the Rho GTPases in the LPA-induced chemotaxis of ovarian cancer cells should be investigated through further experiments, here we first showed the potential roles of RhoA and Rac1, which govern the directional persistence and the migration speed, respectively. In addition, the microfluidic devices, which provide plentiful information not only about the cellular locomotion but also about cell morphology under a stable chemical gradient, would be very useful for such the further studies.

The microfluidics-based approach requires only a few microliters of gels, media solutions, and reagents for the chemotaxis assays. In addition, we could collect the data of individual cells in a high-throughput manner on the basis of automated analysis of time-lapsed images obtained from a live cell imaging system. The microfluidic devices which have multilevel channels for forming a 3D gel structure were fabricated by molding PDMS with stacked adhesive tapes without any cleanroom facilities. This rapid prototyping method allows us to conduct the on-chip chemotaxis assays in conventional biology laboratories without any huge and expensive equipment for fabrication and fluidic manipulation. Compared with the traditional *in vitro* cell migration assays, the microfluidic platform for cell migration assays allows separate quantitative analysis of multiple parameters related to the cell migration, while the traditional methods provide only the unified information about the cell migration. For example, we cannot clearly find out which parameter between the mobility and the directionality affects the increased number of migrated

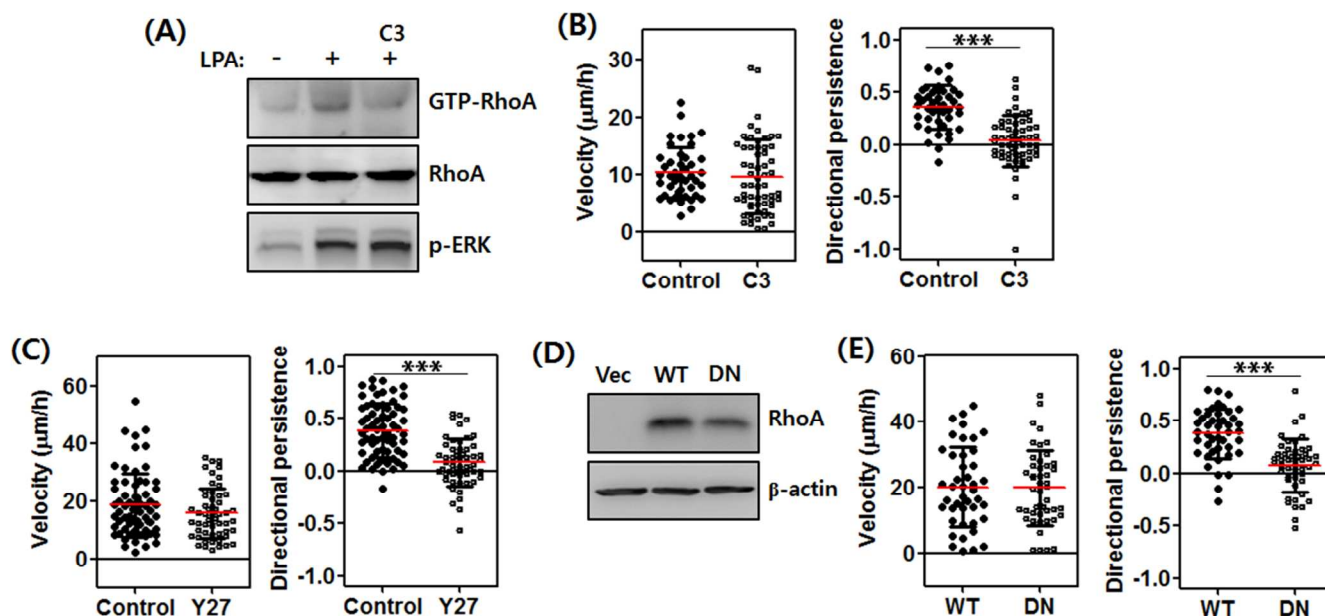


**Fig. 5** Role of RhoA in LPA-induced chemotaxis of SKOV3 cells. (A) Significant reduction in RhoA activity was observed in the cells pretreated with 10 nM C3 exoenzyme (C3) before the addition of 10 µM LPA. Effect of the pretreatment with (B) 10 nM C3 exoenzyme and (C) 10 µM Y-27632 on the average migration speed (left) and the directional persistence (right) of the SKOV3 cells under the LPA concentration gradient across the collagen gel in the microfluidic device. (D) Western blot determination of total RhoA in lysates from the wild-type SKOV3 cells, and the cells transfected with empty vector and dominant-negative N17RhoA. (E) The average migration speed (left) and the directional persistence (right) of the wild-type and the dominant-negative cells in the microfluidic device. \*\*\* $p < 0.0001$ . (C3, 10 nM C3 exoenzyme; Y27, 10 µM Y-27632; Vec, empty vector; WT, wild-type; DN, dominant-negative mutant)

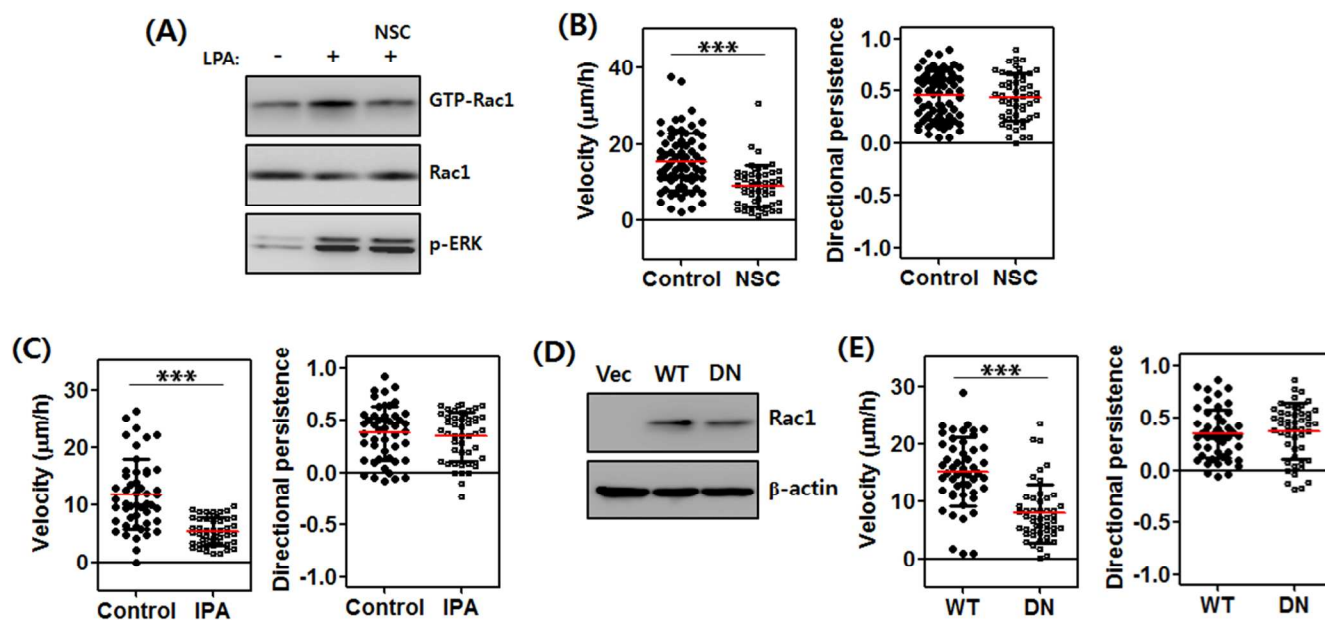


**Fig. 6** Role of Rac1 in LPA-induced chemotaxis of SKOV3 cells. (A) Significant reduction in Rac1 activity was observed in the cells pretreated with 2  $\mu$ M NSC23766 before the addition of 10  $\mu$ M LPA. Effect of the pretreatment with (B) 2  $\mu$ M NSC23766 (NSC) and (C) 2  $\mu$ M IPA-3 (IPA) on the average migration speed (left) and the directional persistence (right) of the SKOV3 cells under the LPA concentration gradient across the collagen gel in the microfluidic device. (D) Western blot determination of total Rac1 in lysates from the wild-type SKOV3 cells, and the cells transfected with empty vector and dominant-negative N17Rac1. (E) The average migration speed (left) and the directional persistence (right) of the wild-type and the dominant-negative cells in the microfluidic device. \*\*\* $p$  < 0.0001. (NSC, 2  $\mu$ M NSC23766; IPA, 2  $\mu$ M IPA-3; Vec, empty vector; WT, wild-type; DN, dominant-negative mutant)

cells in the transwell-based assays. Also, we can neither decouple the information about cellular proliferation and migration nor get any data related to the directionality of cells under stable chemical gradient in the wound-healing assays.

Furthermore, most cell migration studies have been conducted in 2D monolayer format in the traditional methods. However, it has been reported that the protein expression patterns and the effect of anti-cancer drugs in 3D cell culture platforms are significantly different from those in 2D monolayer culture according to recent literature.<sup>49,50</sup> Therefore, our 3D microfluidics-based approach might be essential for revealing mechanism of cancer cell migration. As a consequence, our approach based on live cell imaging and rapid prototyped multilevel microfluidic devices would provide a rapid, low cost, easy-to-use, and versatile way for cell migration studies based on the information that could not be obtained by using the traditional methods such as transwell and wound healing assays.

Understanding the underlying mechanisms of cancer cell migration allows more chances to design anti-migratory compounds, which is one of promising approaches for cancer treatment.<sup>51-53</sup> The microfluidic tools combined with adapted image analysis technologies would provide direct quantitative information on the effects of various compounds on the migration of cancer cells. Despite limitations of *in vitro* studies, the advanced technologies for constructing physiologically relevant *in vitro* tissue microenvironment could open a new era of cancer diagnostics and treatment.

### Acknowledgements

This work was supported by the National Research Foundation of Korea (NRF) grant funded by the Korean government (No.2010-0028684) and a grant of the Korean Health

Technology R&D Project, Ministry of Health & Welfare, Republic of Korea. (A121994).

### Notes and references

<sup>a</sup> School of Nano-Bioscience and Chemical Engineering, Ulsan National Institute of Science and Technology (UNIST), Ulsan, South Korea, [pgsuh@unist.ac.kr](mailto:pgsuh@unist.ac.kr), [ykcho@unist.ac.kr](mailto:ykcho@unist.ac.kr), +82 52 217 2511

‡These authors contributed equally to this work

1. G. B. Mills and W. H. Moolenaar, *Nat. Rev. Cancer*, 2003, **3**, 582-591.
2. Y. Xu, D. C. Gaudette, J. D. Boynton, A. Frankel, X.-J. Fang, A. Sharma, J. Hurteau, G. Casey, A. Goodbody, A. Mellors, B. J. Hobub and G. B. Mills, *Clin. Cancer Res.*, 1995, **1**, 1223-1232.
3. Y. Xu, Z. Shen, D. W. Wiper, M. Wu, R. E. Morton, P. Elson, A. W. Kennedy, J. Belinson, M. Markman and G. Casey, *JAMA*, 1998, **280**, 719-723.
4. Y. Xu, X.-J. Fang, G. Casey and G. B. Mills, *Biochem. J.*, 1995, **309**, 933-940.
5. S. Sengupta, Y.-J. Xiao and Y. Xu, *FASEB J.*, 2003, **17**, 1570-1572.
6. X. Fang, D. Gaudette, T. Furui, M. Mao, V. Estrella, A. Eder, T. Pustilnik, T. Sasagawa, R. Lapushin, S. Yu, R. B. Jaffe, J. R. Wiener, J. R. Erickson and G. B. Mills, *Ann. N. Y. Acad. Sci.*, 2006, **905**, 188-208.
7. J. Ren, Y.-j. Xiao, L. S. Singh, X. Zhao, Z. Zhao, L. Feng, T. M. Rose, G. D. Prestwich and Y. Xu, *Cancer Res.*, 2006, **66**, 3006-3014.
8. T. L. Pua, F. Q. Wang and D. A. Fishman, *Future Oncol.*, 2009, **5**, 1659-1673.

9. T. B. Pustilnik, V. Estrella, J. R. Wiener, M. Mao, A. Eder, M. A. Watt, R. C. B. Jr and G. B. Mills, *Clin. Cancer Res.*, 1999, **5**, 3704-3710.
10. D. A. Fishman, Y. Liu, S. M. Ellerbroek and M. S. Stack, *Cancer Res.*, 2001, **61**, 3194-3199.
11. D. Bian, S. Su, C. Mahanivong, R. K. Cheng, Q. Han, Z. K. Pan, P. Sun and S. Huang, *Cancer Res.*, 2004, **64**, 4209-4217.
12. J. Symowicz, B. P. Adley, M. M. M. Woo, N. Auersperg, L. G. Hudson and M. S. Stack, *Cancer Res.*, 2005, **65**, 2234-2242.
13. S. Sengupta, K. S. Kim, M. P. Berk, R. Oates, P. Escobar, J. Belinson, W. Li, D. J. Lindner, B. Williams and Y. Xu, *Oncogene*, 2007, **26**, 2894-2901.
14. J. So, J. Navari, F.-Q. Wang and D. A. Fishman, *Gynecol. Oncol.*, 2004, **95**, 314-322.
15. J. So, F. Q. Wang, J. Navari, J. Schreher and D. A. Fishman, *Gynecol. Oncol.*, 2005, **97**, 870-878.
16. D. Bian, C. Mahanivong, J. Yu, S. M. Frisch, Z. K. Pan, R. D. Ye and S. Huang, *Oncogene*, 2006, **25**, 2234-2244.
17. E.-K. Kim, J.-M. Park, S. Lim, J. W. Cho, H. S. Kim, H. Seok, J. K. Seo, K. Oh, D.-s. Lee, K. T. Kim, S. H. Ryu and P.-G. Suh, *J. Biol. Chem.*, 2011, **286**, 24036-24045.
18. K. Sawada, K.-i. Morishige, M. Tahara, Y. Ikebuchi, R. Kawagishi, K. Tasaka and Y. Murata, *Gynecol. Oncol.*, 2002, **87**, 252-259.
19. N. Sugimoto, N. Takuwa, K. Yoshioka and Y. Takuwa, *Exp. Cell Res.*, 2006, **312**, 1899-1908.
20. S. Etienne-Manneville and A. Hall, *Nature*, 2002, **420**, 629-635.
21. M. Fukata, M. Nakagawa and K. Kaibuchi, *Curr. Opin. Cell Biol.*, 2003, **15**, 590-597.
22. A. J. Ridley, *J. Cell Sci.*, 2001, **114**, 2713-2722.
23. A. Malliri and J. G. Collard, *Curr. Opin. Cell Biol.*, 2003, **15**, 583-589.
24. M. Parri and P. Chiarugi, *Cell Commun. Signal.*, 2010, **8**, 23.
25. H. Wang, H. Linghu, J. Wang, Y.-l. Che, T.-x. Xiang, W.-x. Tang and Z.-w. Yao, *Tumor Biol*, 2010, **31**, 59-67.
26. K. J. Jeong, S. Y. Park, K. H. Cho, J. S. Sohn, J. Lee, Y. K. Kim, J. Kang, C. G. Park, J. W. Han and H. Y. Lee, *Oncogene*, 2012, **31**, 4279-4289.
27. W. E. Allen, D. Zicha, A. J. Ridley and G. E. Jones, *J. Cell Biol.*, 1998, **141**, 1147-1157.
28. R. Pankov, Y. Endo, S. Even-Ram, M. Araki, K. Clark, E. Cukierman, K. Matsumoto and K. M. Yamada, *J. Cell Biol.*, 2005, **170**, 793-802.
29. B. Wojciack-Stothard and A. J. Ridley, *J. Cell Biol.*, 2003, **161**, 429-439.
30. H. Hwang, J. Park, C. Shin, Y. K. Do and Y.-K. Cho, *Biomed. Microdev.*, 2013, **15**, 627-634.
31. S.-Y. Cheng, S. Heilman, M. Wasserman, S. Archer, M. L. Shuler and M. Wu, *Lab Chip*, 2007, **7**, 763-769.
32. J. Diao, L. Young, S. Kim, E. A. Fogarty, S. M. Heilman, P. Zhou, M. L. Shuler, M. Wu and M. P. DeLisa, *Lab Chip*, 2006, **6**, 381-388.
33. W. Saadi, S. W. Rhee, F. Lin, B. Vahidi, B. G. Chung and N. L. Jeon, *Biomed. Microdev.*, 2007, **9**, 627-635.
34. A. Shamloo, N. Ma, M.-m. Poo, L. L. Sohn and S. C. Heilshorn, *Lab Chip*, 2008, **8**, 1292-1299.
35. U. Haessler, M. Pisano, M. Wu and M. A. Swartz, *Proc. Natl. Acad. Sci. U.S.A.*, 2011, **108**, 5614-5619.
36. E. K. Sackmann, E. Berthier, E. W. K. Young, M. A. Shelef, S. A. Wernimont, A. Huttenlocher and D. J. Beebe, *Blood*, 2012, **120**, e45-e53.
37. E. Berthier, J. Surfus, J. Verbsky, A. Huttenlocher and D. Beebe, *Integr. Biol.*, 2010, **2**, 630-638.
38. L. Liu, Y.-D. Wang, J. Wu, J. Cui and T. Chen, *BMC Cancer*, 2012, **12**, 154.
39. N. Annabi, J. W. Nichol, X. Zhong, C. Ji, S. Koshy, A. Khademhosseini and F. Dehghani, *Tissue Eng Part B Rev.*, 2010, **16**, 371-383.
40. A. Schmidt and A. Hall, *Genes Dev.*, 2002, **16**, 1587-1609.
41. F. N. v. Leeuwen, C. Olivo, S. Grivell, B. N. G. Giepmans, J. G. Collard and W. H. Moolenaar, *J. Biol. Chem.*, 2003, **278**, 400-406.
42. Y. Fukata, M. Amano and K. Kaibuchi, *Trends Pharmacol. Sci.*, 2001, **22**, 32-39.
43. I. Abécassis, B. Olofsson, M. Schmid, G. Zalzman and A. Karniguian, *Exp. Cell Res.*, 2003, **291**, 363-376.
44. G. Totsukawa, Y. Yamakita, S. Yamashiro, D. J. Hartshorne, Y. Sasaki and F. Matsumura, *J. Cell Biol.*, 2000, **150**, 797-806.
45. H. Miki, H. Yamaguchi, S. Suetsugu and T. Takenawa, *Nature*, 2000, **408**, 732-735.
46. B. Knight, C. Laukaitis, N. Akhtar, N. A. Hotchin, M. Edlund and A. R. Horwitz, *Curr. Biol.*, 2000, **10**, 576-585.
47. F. Kheradmand, E. Werner, P. Tremble, M. Symons and Z. Werb, *Science*, 1998, **280**, 898-902.
48. Y. Zhuge and J. Xu, *J. Biol. Chem.*, 2001, **276**, 16248-16256.
49. C. S. Szot, C. F. Buchanan, J. W. Freeman and M. N. Rylander, *Biomaterials*, 2011, **32**, 7905-7912.
50. D. Yip and C. H. Cho, *Biochem. Biophys. Res. Commun.*, 2013, **433**, 327-332.
51. N. Ramnath and P. J. Creaven, *Curr. Oncol. Rep.*, 2004, **6**, 96-102.
52. G. V. Glinisky, *Cancer Metastasis Rev.*, 1998, **17**, 177-185.
53. W. K. Rust, S. W. Carper and G. E. Plopper, *J. Biomed. Biotechnol.*, 2002, **2**, 124-130.